Laminar fluid flow and heat transfer in an annulus with an externally enhanced inner tube

Ajay K. Agrawal
Department of Mechanical Engineering, Clemson University, Clemson, SC, USA

Subrata Sengupta
College of Engineering, University of Michigan, Dearborn, MI, USA

Laminar forced convection in a double-pipe heat exchanger is studied numerically. In this study, an isothermal tube with periodic enhancements (promoters) is placed concentrically inside an insulated circular tube. Pressure drop and heat transfer characteristics of promoters are obtained at various geometric and flow conditions. These are compared to an unenhanced (circular) tube annulus of identical length and heat transfer surface area while the mass flow rate and the Reynolds number are kept the same. A promoter with Gaussian shape establishes superiority over a cosine shape and other normal distribution shapes, since it provides high heat transfer enhancement with a small increase in the pressure drop. Effects of promoter length and spacing on the pressure drop and heat transfer are small. The pressure drop is influenced significantly by the promoter height and the annular gap, while the promoter height is the only significant geometric parameter affecting the heat transfer. At Reynolds numbers of less than 500, the pressure drop in the enhanced tube annulus is 50 percent more than that in the unenhanced tube annulus. Heat transfer enhancement, though small (about 20 percent) at a Peclet number (Re_D Pr) less than 200, increases with the Reynolds number and the Prandtl number. At the highest Re_D (= 1,000) and Pr (= 5) investigated, heat transfer from the enhanced tube annulus is about eight times more than that from the unenhanced tube annulus. However, for this case the pressure drop increases by only a factor of two.

Keywords: augmentation and enhancement; flow separation; forced convection

Introduction

Enhanced surfaces are used in a heat exchanger to obtain compact and less expensive equipment, to decrease its operating cost, or both. Rough or extended surfaces are most common because they require no external power during operation. In commonly used two-fluid tubular heat exchangers, enhancement may be desirable on the inside, the outside, or both sides of the tube. The augmentation is most effective if it is applied to the fluid side offering dominant thermal resistance. Enhancement on the single-phase fluid side is often very important because of the low heat transfer coefficient. Several geometries have been used for single-phase enhancement inside tubes as discussed by Webb (1987).

Longitudinal flow over rod(s) was of interest for gas-cooled reactors and other heat exchangers. For these applications, heat transfer augmentation by rough or extended surfaces is well established in turbulent flow (Dalle Donne and Meyer, 1978; Obermeier and Schaber, 1978; Meyer, 1982). The present work is limited to laminar flow. In both laminar and turbulent flows, enhanced surfaces influence the heat transfer by affecting the flow pattern. Additionally, in turbulent flow, rough or extended surfaces also act as turbulence promoters, since they interrupt the formation of the viscous sublayer on the wall. However, because of different mechanisms at work, the performance characteristics of the enhanced surfaces are not the same in laminar and turbulent flows.

Effects of the external enhancement on laminar flow and heat transfer in a double-pipe heat exchanger were studied numerically by Prata and Sparrow (1984). Periodic enhancement on the inner tube of the annulus offered a good compromise between increases in the pressure drop and the heat transfer. At a Reynolds number of 1,000 and a Prandtl number of 10, the heat transfer increased by a factor of four with an increase in the pressure drop by only a factor of two. The study by Prata and Sparrow (1984) was aimed at a particular geometry, and no attempt was made to optimize the geometric parameters of the enhancement. The present study is extended to include the effects of the enhancement shape, its height and length, the spacing between enhancements, and the annular gap. Optimum geometric parameters are obtained for a shape providing a good compromise between increases in the pressure drop and the heat transfer. Effects of the Reynolds number and the

Address reprint requests to Prof. Agrawal at the Dept. of Mechanical Engineering, Clemson University, Clemson, SC 29634-0921, USA.

Received 26 February 1992; accepted 24 June 1992

Prandtl number are studied for an optimized enhancement shape. Resulting data are correlated to predict the pressure drop and the heat transfer in an enhanced tube annuli.

Formulation of the problem

General description

Figure 1 shows the geometry and the coordinate system of an externally enhanced tube placed inside a circular tube. Axisymmetric promoters on the inner tube are periodic. Each cycle consists of an enhanced and an unenhanced section. Geometric parameters of the enhancement are shape, height (h) and length (L), spacing between promoters, S (or cycle length $L_t = L + S$), and radius ratio of the annulus, γ (or annular gap, $G = 1 - \gamma$). Because of enhancement, the flow cross section varies periodically in the streamwise direction. In experiments with periodically interrupted parallel-plate channels, Berner et al. (1984) observed periodically fully developed flow after an initial distance of a few cycles for flow development. In view of the relatively short entrance region of passages with periodically varying flow cross section, the present work is limited to the periodically fully developed region. In formulating the problem, the following assumptions are made:

(1) the flow is laminar;
(2) the fluid with constant properties is Newtonian and incompressible;
(3) the viscous dissipation is negligible; and
(4) the flow geometry is axisymmetric.

The physical domain for computations is the symmetry region A-B-C-D shown in Figure 1. Since the flow is periodically fully developed, any two cross-sectional planes at a distance of L_t from one another could be used as inflow and outflow boundaries. The region A-B-C-D in Figure 1 was chosen to help present the results.

Flow field

Navier–Stokes equations are expressed in the vorticity-stream function form. Governing equations in the axisymmetric cylindrical coordinates are nondimensionalized and are written as follows.

Notation

A_s	Heat transfer surface area, Equation 17, m^2
$C0$, $C1$	Geometric coefficients, Equations 22–23
$C2$	Constant in Equation 25
c_p	Specific heat of the fluid, J/kg K
D_h^*	Hydraulic diameter, Equation 13, m
EI	Efficiency index, $[R_{\overline{Nu}}/R_{\Delta P}]$
G	Annular gap, $[1 - \gamma]$
h	Promoter height
h_w	Local heat transfer coefficient, Equation 12, W/m^2 K
$\bar{h}$	Average heat transfer coefficient, Equation 15, W/m^2 K
k	Thermal conductivity, W/mK
L	Length of the promoter
L_t	Periodic length of the promoter, $[L + S]$
$\dot{m}$	Mass flow rate, kg/s
Nu	Local Nusselt number, Equation 11
$\overline{Nu}$	Average Nusselt number in an enhanced tube annulus
$\overline{Nu_a}$	Average Nusselt number in an unenhanced tube annulus
n	Normal to the wall
np	Integer in Equation 25
P	Pressure, $[P^*/\rho w_m^2]$
ΔP	Total pressure drop in an enhanced tube annulus
ΔP_a	Total pressure drop in an unenhanced tube annulus
Pe	Peclet number, [Re Pr]
Pr	Prandtl number, $[\mu c_p/k]$
$\dot{Q}$	Net heat transfer rate, Equation 16, W
Re	Reynolds number based upon the outer tube radius, $[w_m r_2^*/\nu]$
Re_D	Reynolds number based upon the hydraulic diameter, $[w_m D_h^*/\nu]$
$R_{\overline{Nu}}$	Average Nusselt number ratio, $[\overline{Nu}/\overline{Nu_a}]$
$R_{\Delta P}$	Total pressure drop ratio, $[\Delta P/\Delta P_a]$
r	Radial coordinate
r_e	Equivalent radius, Equation 5
r_i^*	Radius at unenhanced section of the inner tube, m
$r_1(Z)$	Inner tube radius, Equations 24–25
r_2^*	Outer tube radius, m
S	Spacing between promoters
T	Temperature, $[T^* - T_{o1}^*]/[T_{i1}^* - T_{o1}^*]$
T_m	Mean temperature, Equation 10
ΔT_m^*	Mean temperature difference, Equation 18, K
u	Radial velocity
w	Axial velocity
w_m	Mean axial velocity, m/s
x_l	Length of the lower eddy
x_{rl}	Reattachment point of the lower eddy
x_{ru}	Reattachment point of the upper eddy
x_{sl}	Separation point of the lower eddy
x_{su}	Separation point of the upper eddy
x_u	Length of the upper eddy
Z	Axial coordinate

Greek symbols

β	Axial coordinate in the transformed domain
γ	Radius ratio, $[r_i^*/r_2^*]$
η	Radial coordinate in the transformed domain
θ	Nondimensional temperature, Equation 9
ν	Kinematic viscosity, m^2/s
ρ	Density, kg/m^3
ψ	Stream function
ψ_l	Strength of the lower eddy, $[(\psi_{max} - \psi_i)/\psi_i]$
ψ_u	Strength of the upper eddy, $[\lvert\psi_{min}\rvert/\psi_i]$
Ω	Vorticity

Subscripts and superscripts

1	Inlet
2	Outlet
i	Inner wall
o	Outer wall
*	Dimensional quantity

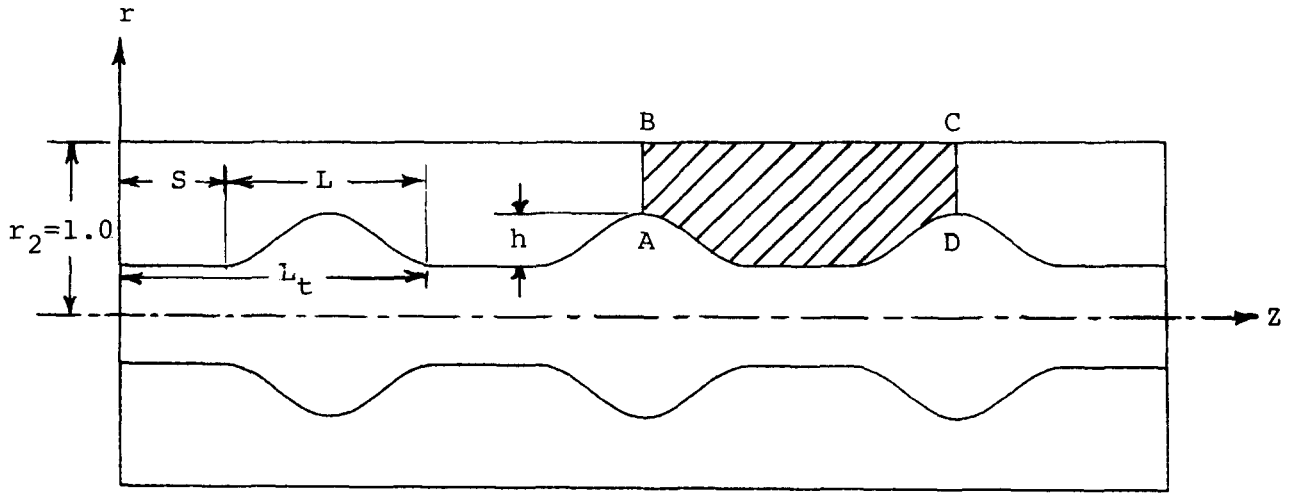

Figure 1 Geometric representation of an annulus with an externally enhanced inner tube

Vorticity transport equation

$$\frac{\partial}{\partial r}(u\Omega)+\frac{\partial}{\partial Z}(w\Omega)=\frac{1}{\mathrm{Re}}\left[\frac{\partial^2\Omega}{\partial r^2}+\frac{\partial^2\Omega}{\partial Z^2}+\frac{1}{r}\frac{\partial\Omega}{\partial r}-\frac{\Omega}{r^2}\right] \tag{1}$$

Vorticity definition equation

$$\frac{1}{r}\frac{\partial^2\psi}{\partial r^2}+\frac{1}{r}\frac{\partial^2\psi}{\partial Z^2}-\frac{1}{r^2}\frac{\partial\psi}{\partial r}=\Omega \tag{2}$$

Stream function definition equations

$$u=\frac{1}{r}\frac{\partial\psi}{\partial Z} \tag{3a}$$

$$w=-\frac{1}{r}\frac{\partial\psi}{\partial r} \tag{3b}$$

In Equations 1 to 3, all space variables and flow quantities are nondimensionalized with respect to the outer tube radius, r_2^*, and the mean axial velocity, w_m, respectively. Other quantities are defined as follows:

$$\psi=\frac{\psi^*}{w_m r_2^{*2}},\quad \Omega=\frac{\Omega^* r_2^*}{w_m},\quad \mathrm{Re}=\frac{w_m r_2^*}{\nu}$$

Boundary conditions. Stream function values at the walls determine the mass flow rate in the annular passage. At the outer tube wall, the stream function value is specified as zero ($\psi_o = 0$). At the inner tube wall, the stream function value is

$$\psi_i=(1-r_e^2)/2 \tag{4}$$

which corresponds to the volume flow rate in an annulus with a circular inner tube of radius r_e, providing the same surface area as the enhanced inner tube. The equivalent radius, r_e, is expressed as

$$r_e=\left[\int_0^{L_t} r_1(Z)\sqrt{\left\{1+\left(\frac{dr_1}{dZ}\right)^2\right\}}\,dZ\right]\Big/ L_t \tag{5}$$

Vorticity boundary conditions at the solid walls are obtained from Equation 2, which requires stream function values other than those at the walls. Therefore, the wall vorticity is obtained iteratively. Because of the periodic nature of the flow, stream function and vorticity values are the same at the inlet and the outlet.

Pressure distribution

Pressure distribution is obtained along the outer tube wall. With $u = 0$ and $w = 0$ at the wall, the axial momentum equation results in

$$\left.\frac{dP}{dZ}\right|_o=\frac{1}{\mathrm{Re}}\left[\frac{\partial^2 w}{\partial r^2}+\frac{1}{r}\frac{\partial w}{\partial r}\right]\qquad \text{at } r=r_2=1.0 \tag{6}$$

where pressure, P, has been nondimensionalized with respect to ρw_m^2. Using Equations 2 and 3, Equation 6 is written as

$$\left.\frac{dP}{dZ}\right|_o=\frac{1}{\mathrm{Re}}\left[\frac{\partial^2 u}{\partial r\partial Z}-\frac{1}{r}\frac{\partial}{\partial r}(r\Omega)\right] \tag{7}$$

Pressure distribution along the outer tube wall is obtained by integrating Equation 7 in the axial direction. For reference, the inlet pressure is specified as zero.

Temperature field

The energy equation is written as

$$\frac{\partial}{\partial r}(uT)+\frac{\partial}{\partial Z}(wT)=\frac{1}{\mathrm{Pe}}\left[\frac{\partial^2 T}{\partial r^2}+\frac{\partial^2 T}{\partial Z^2}+\frac{1}{r}\frac{\partial T}{\partial r}\right]-\frac{uT}{r} \tag{8}$$

where the temperature, T, has been nondimensionalized with respect to the wall temperature difference at the inlet, i.e., $T=[T^*-T_{o1}^*]/[T_{i1}^*-T_{o1}^*]$.

Boundary conditions. Thermal boundary conditions at the walls are constant temperature at the inner tube ($T_i = 1.0$) and insulated outer tube ($\partial T/\partial n|_o = 0$). In the periodically fully developed region, the temperature field, θ, defined as

$$\theta=\frac{T-T_i}{T_m-T_i} \tag{9}$$

is the same at the inlet and the outlet. The bulk temperature, T_m, in Equation 9 is defined as

$$T_m=\frac{\int_{r_1(Z)}^1 Twrdr}{\int_{r_1(Z)}^1 wrdr} \tag{10}$$

Thermal boundary conditions at the inlet and the outlet are not known explicitly. A procedure described by Kelkar and Patankar (1987) has been used in the present study whereby the temperature boundary conditions are derived from the θ boundary conditions.

Nusselt number definitions. The local Nusselt number is defined as

$$\mathrm{Nu} = h_w D_h^*/k \tag{11}$$

where the local heat transfer coefficient, h_w, is obtained from the local heat balance, and D_h^* is the hydraulic diameter:

$$h_w = -k\left.\frac{\partial T}{\partial n^*}\right|_{r_1^*} \Big/ (T_w - T_m) \tag{12}$$

$$D_h^* = 2r_2^*(1 - r_e) \tag{13}$$

The average Nusselt number is defined as

$$\overline{\mathrm{Nu}} = \bar{h} D_h^*/k \tag{14}$$

where the average heat transfer coefficient, $\bar{h}$, is obtained from the overall heat balance:

$$\bar{h} = \dot{Q}/(A_s \Delta T_m^*) \tag{15}$$

Quantities in Equation 15 are the net heat transfer rate, $\dot{Q}$, the heat transfer surface area, A_s, and the mean temperature difference, ΔT_m^*, given as

$$\dot{Q} = \dot{m} c_p (T_{m2}^* - T_{m1}^*) \tag{16}$$

$$A_s = 2\pi r_e^* L_t^* \tag{17}$$

$$\Delta T_m^* = \Delta T_m = [(T_w - T_{m1}) + (T_w - T_{m2})]/2 \tag{18}$$

where T_{m1} and T_{m2} are bulk temperatures at the inlet and the outlet.

Transformation

Since an axisymmetric coordinate system does not fit the enhanced tube boundaries, the radial coordinate is transformed algebraically to obtain a rectangular computational domain. The transformation is given as

$$\eta = \frac{r - r_1(Z)}{1 - r_1(Z)} \tag{19a}$$

$$\beta = Z \tag{19b}$$

The first gradient terms in the transformed coordinates are

$$\partial/\partial r = C0(\partial/\partial\eta) \tag{20}$$

$$\partial/\partial Z = C1(\partial/\partial\eta) + \partial/\partial\beta \tag{21}$$

where $C0$ and $C1$ are geometric coefficients of transformation given as

$$C0 = 1/[1 - r_1(Z)] \tag{22}$$

$$C1 = \left(\frac{\eta - 1}{1 - r_1(Z)}\right)\frac{dr_1(Z)}{dZ} \tag{23}$$

Equations 19–23 are used to transform the governing and boundary-condition equations. Further details of the transformed equations are given by Agrawal and Sengupta (1989).

Numerical solution

Using the power-law scheme of Patankar (1980), the transformed governing and boundary-condition equations are converted to a set of finite-difference equations. Steady-state results are obtained by including a false time-dependent term in the vorticity and the energy equations. Difference equations are solved using an iterative Alternate Direction Implicit (ADI) scheme described by Agrawal and Sengupta (1989). The steady state is confirmed when the change in the total pressure drop (ΔP) and the average Nusselt number ($\overline{\mathrm{Nu}}$) with timewise iterations is smaller, within 1 percent in about 500 time steps. Approximately 1,500 and 4,000 time steps were required for the vorticity and the energy equations, respectively.

Table 1 Comparison of present computations with those by Prata and Sparrow (1984)

	r_e	x_{sl}	x_{rl}	$R_{\Delta P}$	$\overline{\mathrm{Nu}}$
Prata and Sparrow (1984)	0.552	0.37	1.76	2.65	≈12.5
Present computations	0.552	0.30	1.78	2.44	12.3
Difference				8%	≈3%

Table 2 ΔP and $\overline{\mathrm{Nu}}$ for two different meshes

Grid size	ΔP	$\overline{\mathrm{Nu}}$
31 × 73	1.974	8.666
41 × 91	1.967	8.233

The mathematical model and the computer program were verified using analytical solutions for a concentric circular annulus. Some of these results were presented by Agrawal and Sengupta (1987, 1989). Present computations in an annulus with a periodically enhanced inner tube were compared to those by Prata and Sparrow (1984). The inner tube wall was approximated by a sinusoidal curve, since its exact shape was not prescribed by Prata and Sparrow (1984). The results obtained at $\mathrm{Re}_D = 1{,}000$, $\mathrm{Pr} = 2$ are given in Table 1.

Present predictions of the overall pressure drop and the average Nusselt number compare well with those by Prata and Sparrow (1984). Some differences were attributed to differences in the physical domains used for the two cases.

Grid-size convergence for the present study was checked at the base conditions for a cosine-shape enhancement (described later) with 31 radial, 73 axial (31 × 73) and 41 radial, 91 axial (41 × 91) grid points. Velocity and temperature fields were within 5 percent. The total pressure drop and the average Nusselt number with two different meshes are given in Table 2.

In order to accurately resolve the solution at conditions different from the base case, a 41 × 91 grid was used for all computations. Depending upon flow and geometric parameters, the computations for the flow field required 20 to 150 minutes and that for the energy equation required 15 to 30 minutes on an IBM 3081.

Results and discussions

Flow and temperature fields in the annular passage and pressure distribution along the outer tube are obtained for a range of geometric and flow parameters. Relying on studies by Prata and Sparrow (1984), a base case with the following parameters is selected.

Base conditions

Flow parameters. Reynolds number, $\mathrm{Re}_D = 1{,}000$
Prandtl number, $\mathrm{Pr} = 1$

Geometric parameters. Radius ratio, $\gamma = 0.4$ or annular gap, $G = 0.6$
Promoter height, $h = 0.3$
Promoter length, $L = 1.2$
Plain length, $S = 0.6$
Cycle length, $L_t = L + S = 1.8$

The governing equations (Equations 1 and 8) are written in terms of the Reynolds number based on the outer tube radius (Re_D). These equations are solved at a specified Re_D by using an equivalent Re [$= Re_D r_2^*/D_h^*$ or $0.5\ Re_D/(1 - r_e)$].

Effect of promoter shape

In the first part of the study, performance characteristics of four promoter shapes, shown in Figure 2, were obtained at the base conditions. The radius of the inner tube with these promoters (one cosine and three normal distribution shapes) is given as

$$r_1(Z) = \gamma + h[1 - \cos(2\pi Z/L)] \tag{24}$$

and

$$r_1(Z) = \gamma + h\, e^{-C2|Z-Z0|^{np}} \quad \text{with } np = 2, 3, \text{ and } 4 \tag{25}$$

where $C2 = 4/(L/2)^{np}$ and $Z0 = L/2$.

Performance evaluation. The total pressure drop (ΔP) and the average Nusselt number ($\overline{Nu}$) in an enhanced tube annulus are compared to those in an unenhanced tube annulus (ΔP_a and $\overline{Nu}_a$). For comparison, the cycle length (L_t), the heat transfer surface area (A_s), the mass flow rate ($\dot{m}$), and the Reynolds number (based upon the hydraulic diameter, Re_D) for the two are kept the same. The pressure drop ratio, $R_{\Delta P}$ ($= \Delta P/\Delta P_a$) and the Nusselt number ratio, $R_{\overline{Nu}}$ ($= \overline{Nu}/\overline{Nu}_a$) for various enhancements along with the radius of an equivalent circular tube, r_e, are given in Table 3.

Table 3 Performance characteristics of promoters at base conditions

	Cosine	$np = 2$	$np = 3$	$np = 4$
r_e	0.551	0.541	0.567	0.588
$R_{\Delta P}$	1.967	2.325	2.432	2.389
$R_{\overline{Nu}}$	1.494	2.275	2.228	2.181
EI	0.760	0.978	0.916	0.913

In Table 3 the total pressure drop and the average Nusselt number increase for all enhancement shapes. Heat transfer in the enhanced tube annulus is 50 to 130 percent more than that in an equivalent unenhanced tube annulus. This increase in heat transfer is accompanied with an increase of 95 to 145 percent in the pressure drop. The cosine-shape promoter provides the least amount of heat transfer enhancement. Increase in the pressure drop is also minimum for this shape. Differences among the remaining three shapes are small, within 5 percent of each other.

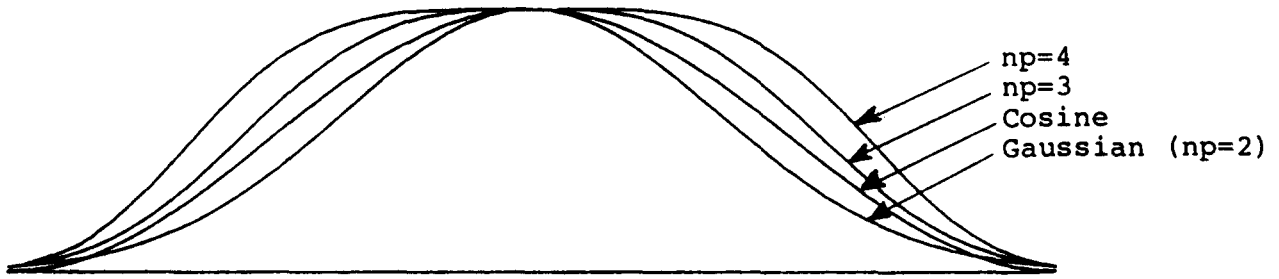

Figure 2 Enhancement shapes

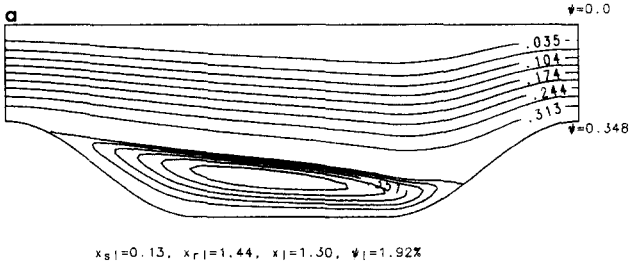

$x_{s|}$=0.13, $x_{r|}$=1.44, $x_{|}$=1.30, $\psi_{|}$=1.92%

Figure 3a Streamline pattern: cosine shape enhancement

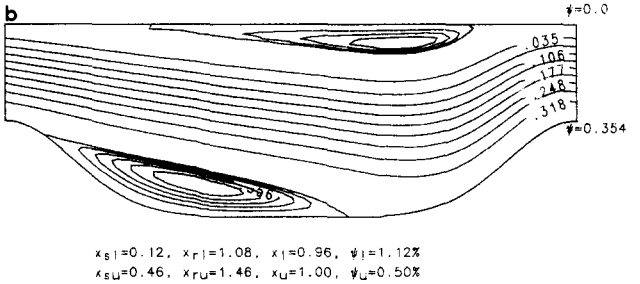

$x_{s|}$=0.12, $x_{r|}$=1.08, $x_{|}$=0.96, $\psi_{|}$=1.12%
x_{su}=0.46, x_{ru}=1.46, x_{u}=1.00, ψ_{u}=0.50%

Figure 3b Streamline pattern: Gaussian shape enhancement ($np = 2$)

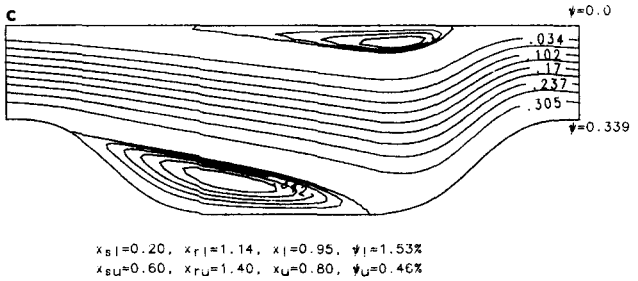

$x_{s|}$=0.20, $x_{r|}$=1.14, $x_{|}$=0.95, $\psi_{|}$=1.53%
x_{su}=0.60, x_{ru}=1.40, x_{u}=0.80, ψ_{u}=0.46%

Figure 3c Streamline pattern: normal distribution shape ($np = 3$)

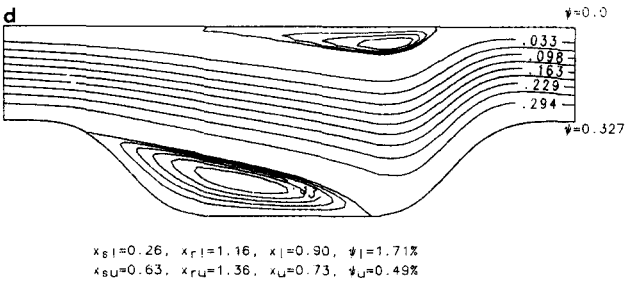

$x_{s|}$=0.26, $x_{r|}$=1.16, $x_{|}$=0.90, $\psi_{|}$=1.71%
x_{su}=0.63, x_{ru}=1.36, x_{u}=0.73, ψ_{u}=0.49%

Figure 3d Streamline pattern: normal distribution shape ($np = 4$)

Performance of a promoter has been evaluated by its efficiency index, EI [$= R_{\overline{Nu}}/R_{\Delta P}$]. High EI means heat transfer enhancement with a small increase in the pressure drop. A desirable promoter is one with a high Nusselt-number ratio as well as a high efficiency index. Such a promoter will result in a high heat transfer and low pressure drop. A promoter with Gaussian shape ($np = 2$) satisfies this criterion (see Table 3). A Gaussian shape promoter provides a 128 percent increase in the heat transfer with a 133 percent increase in the pressure drop, corresponding to EI close to one. In contrast, Rowley and Patankar (1984) found that circumferential fins inside a tube decrease the net heat transfer, except at high Prandtl numbers, even though the pressure drop increases by an order of magnitude. Similar observations were made by Cheng and Huang (1991) for laminar forced convection in parallel-plate channels with staggered and inline transverse fin arrays. Because of its superior performance, the Gaussian promoter has been used subsequently to study the effects of other geometric and flow parameters.

An insight into the effects of the enhancement shape on pressure drop and heat transfer is gained from flow and temperature distributions in the annular domain.

Flow field. Figures 3a to 3d show the streamline pattern in the annular domain for the four enhancements, respectively. For all shapes, the flow field is characterized by a recirculating region in the wake of the promoter. A weak recirculating zone exists also on the outer tube wall for all but the cosine-shape promoter. Locations of separation and reattachment points (x_{sl}, x_{su}, x_{rl}, and x_{ru}), lengths (x_l and x_u), and strengths (ψ_l and ψ_u) of the recirculating eddies are also given in Figures 3a to 3d. Flow fields with normal distribution promoters are similar, yet different from the cosine promoter. This result is attributed to the fact that the cosine-shape promoter changes the flow area somewhat gradually as compared to all other promoters studied. Comparisons between the cosine and Gaussian promoters indicate that the two shapes are almost the same near the inlet, thereby resulting in coincidental separation points. Thereafter, the Gaussian promoter effects a sharper increase in the flow area. As a result, the main flow is accelerated towards the enhanced tube wall, causing early reattachment. A stronger streamline curvature towards the inner tube also enlarges the stagnant region near the outer tube wall and creates a rather weak secondary eddy (ψ_u is only 0.5 percent). For both shapes, the strength of the eddy in the wake of the promoter is low (1.92 and 1.12 percent) compared to the main flow. For other promoters, as np increases, the narrow region of the passage becomes flatter, and the slope thereafter increases. Because the length of the passage with the constant flow area increases, the separation is delayed, i.e., the x_{sl} increases. However, because the steeper change in the flow area increases the flow diversion, the reattachment occurs early. As a result, the size of the recirculation eddy decreases. This is also true for the recirculation eddy on the outer tube wall.

Pressure distributions along the outer tube wall for enhanced and unenhanced tube annuli are shown in Figure 4. A direct comparison of the total pressure drop cannot be made because of different mass flows through various passages; the highest mass flow rate corresponds to the Gaussian promoter (with smallest r_e). Figure 4 shows that for all enhanced tube annuli,

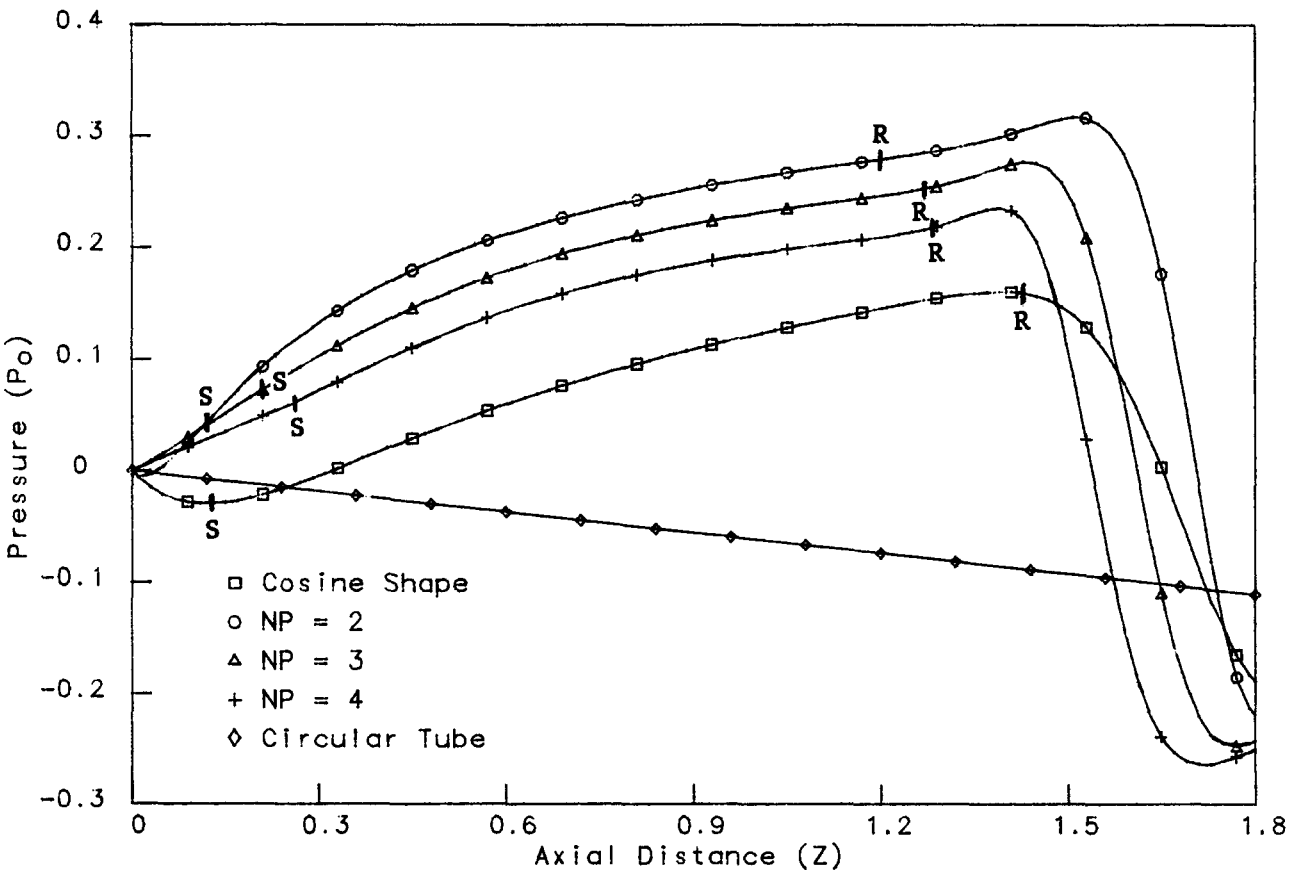

Figure 4 Effect of promoter shape on pressure along the outer tube: $Re_D = 1{,}000$, $G = 0.6$, $h = 0.3$, $L = 1.2$, $S = 0.6$. S: point of separation; R: point of reattachment

the pressure distribution is marked by two distinct regions, those with pressure drop and pressure recovery. Pressure recovery takes place in the recirculating region. Most of the pressure drop occurs after reattachment as the fluid passes through the converging passage. For normal distribution shapes, the pressure gradient in this region is essentially the same, as shown in Figure 4. The total pressure drop is only marginally different. The pressure gradient for the cosine shape is considerably less because of the relatively gradual change in the flow area. For this case, pressure recovery on the outer tube wall is also small. Maximum pressure recovery is achieved with a Gaussian promoter because of a large separated region near the outer wall (x_u is highest for this case). Superior performance of the Gaussian promoter can be attributed to its pressure recovery features.

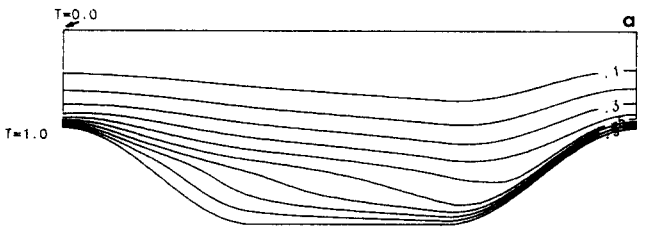

Figure 5a Isotherms: cosine shape promoter. $Re_D = 1{,}000$, $Pr = 1$, $G = 0.6$, $h = 0.3$, $L = 1.2$, $S = 0.6$

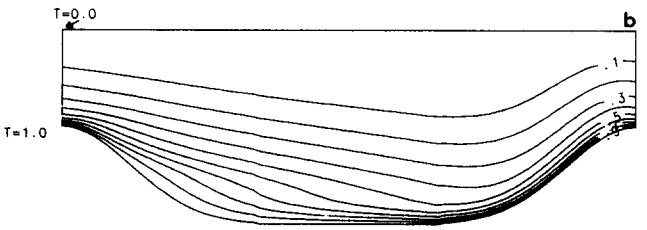

Figure 5b Isotherms: Gaussian shape promoter. $Re_D = 1{,}000$, $Pr = 1$, $G = 0.6$, $h = 0.3$, $L = 1.2$, $S = 0.6$

Temperature field. Figures 5a and 5b show isotherms in the annular domain with cosine and Gaussian promoters, respectively. Isotherm spacing in Figures 5a and 5b indicates that the temperature gradient is high in the narrow region where the axial velocity is highest. With a Gaussian promoter, isotherms in the heated region are more closely spaced (Figure 5b) as compared to those with a cosine promoter (Figure 5a) because of a stronger flow diversion towards the enhanced tube wall. Also, the region of low-temperature fluid near the insulated wall is wider, as indicated by the isotherm corresponding to $T = 0.1$. Isotherms with other shapes were similar to those with a Gaussian promoter.

Local Nusselt numbers along the enhanced tube wall are shown in Figure 6. Also shown is an average value corresponding to the unenhanced tube annulus. In the narrow region, the heat transfer from the enhanced tube is three to four times that from the unenhanced tube. As the flow velocity decreases with increasing flow area, the heat transfer reduces and decreases considerably as the flow separates. Further downstream, the heat transfer increases within the separated region because of a growing reverse boundary layer. A point of maximum heat transfer is obtained after the flow reattaches. Thereafter, the

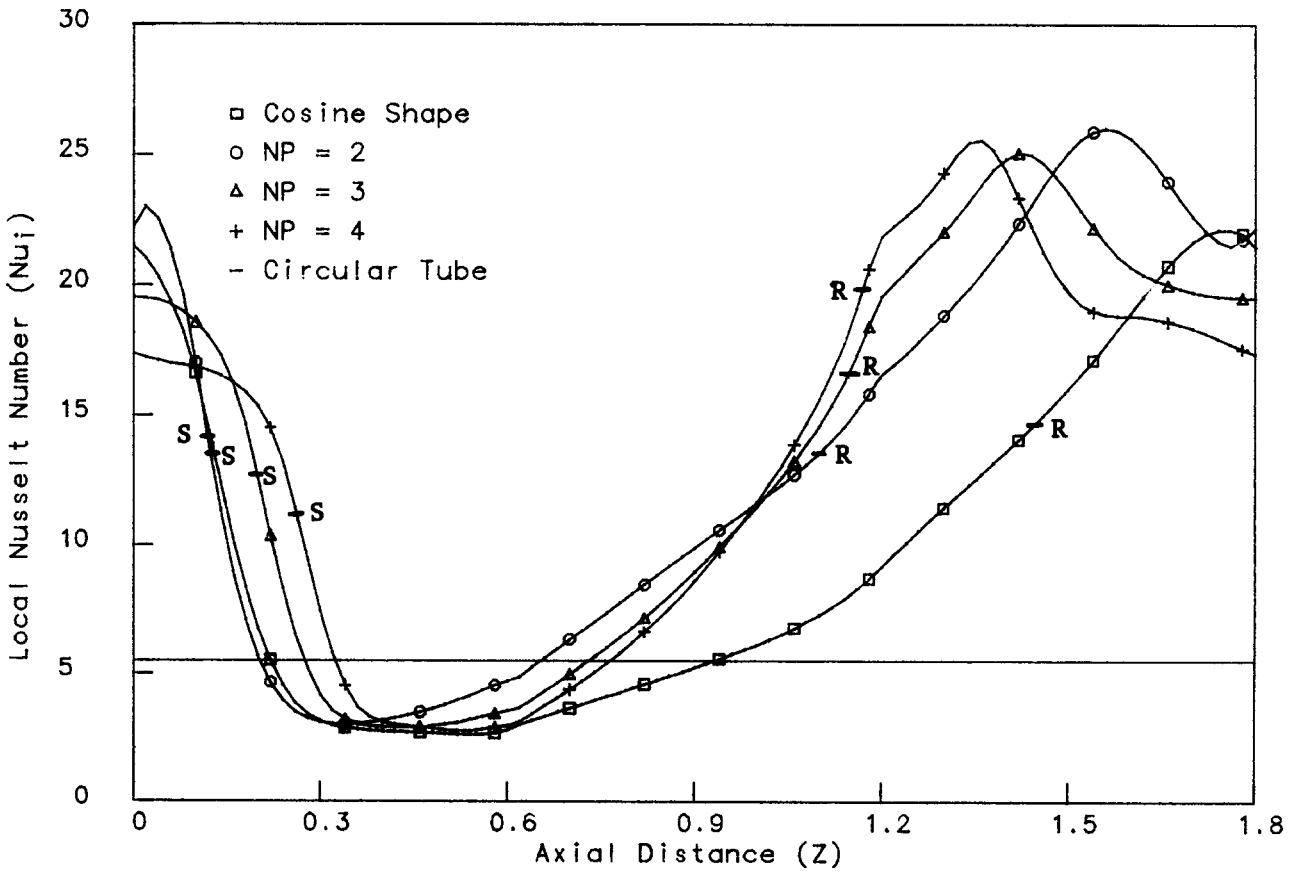

Figure 6 Effect of promoter shape on Nusselt number along the inner tube: $Re_D = 1{,}000$, $Pr = 1$, $G = 0.6$, $h = 0.3$, $L = 1.2$, $S = 0.6$. S: point of separation; R: point of reattachment

Nusselt number decreases as the thermal boundary layer redevelops. Since the $np = 4$ promoter provides the maximum length for boundary-layer development, it results in the minimum Nusselt number at the exit or inlet. In Figure 6, comparisons between cosine and Gaussian shapes indicate that the local Nusselt number for the two is essentially the same until $Z \simeq 0.3$. After that point, the Gaussian promoter causes heat transfer to increase because of the stronger flow diversion towards the heated wall. Remaining promoters also provide comparable heat transfer enhancement, except in the narrow region where the Nusselt number decreases because of boundary-layer development assisted by the flat portion of the promoter.

Effect of geometric parameters (Gaussian promoter)

Promoter height. As shown in Figure 7, both the pressure drop and the heat transfer increase with the promoter height. At a low height, the heat transfer increases with a relatively smaller increase in the pressure drop. However, beyond $h = 0.3$, heat transfer enhancement is accompanied with a much greater pressure-drop penalty. For example, increasing h from 0.3 to 0.4 causes heat transfer to increase by 54 percent; however, the pressure drop increases by 109 percent.

Annular gap. Heat transfer enhancement is only marginally influenced by the annular gap, as shown in Figure 8. On the other hand, the pressure drop increases significantly as the annular gap decreases. It can be inferred that an enhanced tube inside a larger circular tube (corresponding to a smaller radius ratio) provides better heat transfer enhancement. In the present study, an annulus with $G = 0.7$ (i.e., $\gamma = 0.3$) results in the highest EI (= 1.12) as well as high $R_{\overline{Nu}}$ (= 2.22).

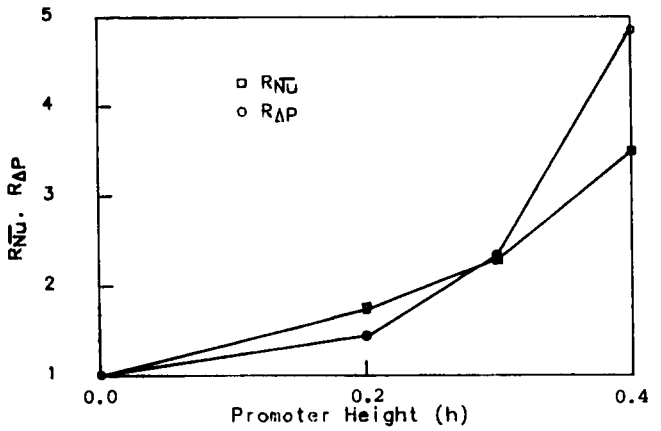

Figure 7 Effect of promoter height at $Re_D = 1{,}000$, Pr = 1, $G = 0.6$, $L = 1.2$, $S = 0.6$

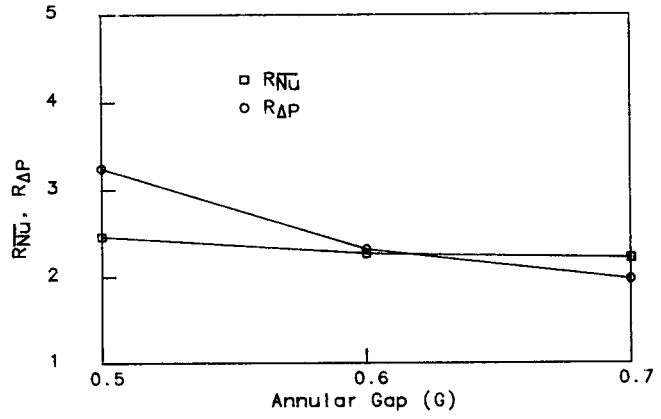

Figure 8 Effect of annular gap at $Re_D = 1{,}000$, Pr = 1, $h = 0.3$, $L = 1.2$, $S = 0.6$

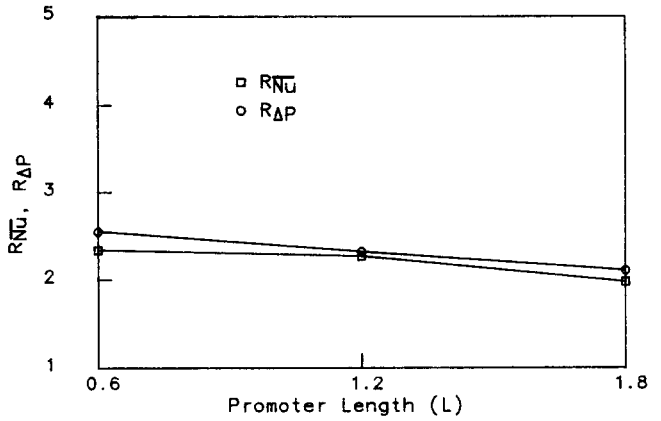

Figure 9 Effect of promoter length at $Re_D = 1{,}000$, Pr = 1, $G = 0.6$, $h = 0.3$, $S = 0.6$

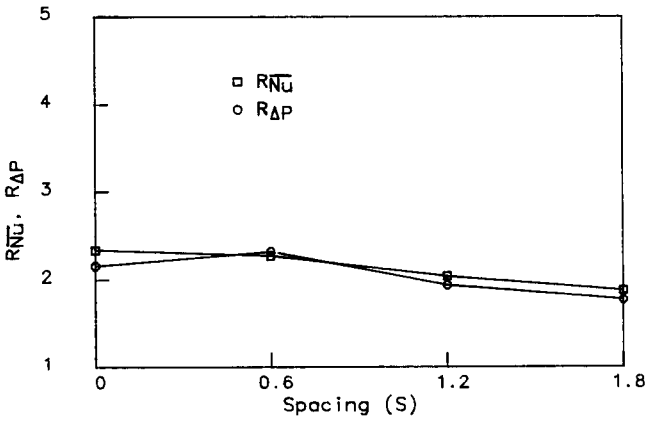

Figure 10 Effect of promoter spacing at $Re_D = 1{,}000$, Pr = 1, $G = 0.6$, $h = 0.3$, $L = 1.2$

Promoter length. Effects of promoter length on the pressure drop and the heat transfer are shown in Figure 9. Heat transfer enhancement due to promoters with $L = 1.2$ and 0.6 is essentially the same. However, the pressure drop is slightly more for the shorter length. At $L > 1.2$, both the heat transfer and the pressure-drop ratios decrease. At all lengths, the pressure-drop ratio is slightly more than the Nusselt-number ratio (i.e., EI < 1). A promoter with $L = 1.2$ provides the best performance.

Promoter spacing. Effects of promoter spacing on the pressure drop and the heat transfer are shown in Figure 10, which is somewhat similar to Figure 9. With increases in spacing, the heat transfer decreases because of the reduction in the enhanced surface area. In general, the pressure drop also decreases. The best compromise is achieved at $S = 0$, i.e., when there is no flat region between the promoters. Resulting values are $R_{\overline{Nu}} = 2.34$, $R_{\Delta P} = 2.16$, and EI = 1.08.

Optimum geometric parameters

From the results described above, optimum geometric parameters are obtained at $Re_D = 1{,}000$ and Pr = 1.0. These are $\gamma = 0.3$ or

Table 4 Performance characteristics of an annulus with externally enhanced inner tube (41 × 91 grid)

Purpose	Re_D	Pr	h	G	L	S	r_e	$R_{\Delta P}$	$R_{\overline{Nu}}$	EI
Base case	1,000	1.0	0.3	0.6	1.2	0.6	0.541	2.33	2.27	0.97
Effect of promoter height	1,000	1.0	0.2	0.6	1.2	0.6	0.481	1.44	1.72	1.19
			0.3				0.541	2.33	2.27	0.97
			0.4				0.614	4.85	3.50	0.72
Effect of annular gap	1,000	1.0	0.3	0.5	1.2	0.6	0.650	2.25	2.47	1.10
				0.6			0.541	2.33	2.27	0.97
				0.7			0.432	1.98	2.22	1.12
Effect of promoter length	1,000	1.0	0.3	0.6	0.6	0.6	0.595	2.55	2.34	0.92
					1.2		0.541	2.33	2.27	0.97
					1.8		0.527	2.11	1.98	0.94
Effect of promoter spacing	1,000	1.0	0.3	0.6	1.2	0.0	0.611	2.16	2.34	1.08
						0.6	0.541	2.33	2.27	0.97
						1.2	0.506	1.94	2.04	1.05
						1.8	0.485	1.77	1.88	1.06
Optimum geometric parameters	1,000	1.0	0.3	0.7	1.2	0.0	0.497	2.06	2.39	1.16
Effect of Reynolds number	100	1.0	0.3	0.7	1.2	0.0	0.497	1.43	1.14	0.71
	200							1.42	1.21	0.85
	500							1.53	1.63	1.07
	1,000							2.06	2.39	1.16
Effect of Prandtl number	100	0.7	0.3	0.7	1.2	0.0	0.497	1.43	1.17	0.82
		1.0						1.43	1.14	0.80
		2.0						1.43	1.20	0.84
		5.0						1.43	1.61	1.13
	200	0.7	0.3	0.7	1.2	0.0	0.497	1.42	1.16	0.82
		1.0						1.42	1.21	0.85
		2.0						1.42	1.48	1.04
		5.0						1.42	2.44	1.72
	500	0.7	0.3	0.7	1.2	0.0	0.497	1.53	1.39	0.91
		1.0						1.53	1.63	1.07
		2.0						1.53	2.43	1.59
		5.0						1.53	4.79	3.13
	1,000	0.7	0.3	0.7	1.2	0.0	0.497	2.06	1.91	0.93
		1.0						2.06	2.39	1.16
		2.0						2.06	4.00	1.94
		5.0						2.06	8.65	4.20

$G = 0.7$, $h = 0.3$, $L = 1.2$, and $S = 0$ or $L_t = 1.2$. With these geometric parameters, $R_{\Delta P} = 2.06$, $R_{\overline{Nu}} = 2.39$, and EI = 1.16 are obtained. These values represent a performance superior to all other promoters studied.

Effect of flow parameters (at G = 0.7, h = 0.3, L = 1.2, and S = 0.0)

Effects of the Reynolds number and the Prandtl number on the overall performance of the promoter are shown in Figure 11 (on log–log scale). The pressure drop is independent of the Prandtl number. The pressure-drop ratio is nearly constant ($\simeq 1.5$) for $Re_D < 500$. Heat transfer enhancement, though small (about 20 percent) at Re_D Pr < 200, increases with Re_D and Pr. At the highest Re_D (= 1,000) and Pr (= 5) investigated, the heat transfer in an enhanced tube annulus is nearly eight times higher than that in an unenhanced tube annulus. For this case, the pressure drop increases only by a factor of two.

Correlation of data

The Nusselt-number ratio and the pressure-drop ratio are useful design tools. In the present study, a total of 26 runs were made by varying geometric and flow parameters for an enhancement with Gaussian shape (see Table 4). $R_{\Delta P}$ and $R_{\overline{Nu}}$ from these runs were correlated using multiple linear regression. These correlations are given below.

Pressure-drop ratio

$$R_{\Delta P} = 1 + \frac{0.000162 Re_D^{0.382}}{(L)^{0.08}(L_t)^{0.42}(1-h)^{7.55}(G)^{2.97}} \tag{26}$$

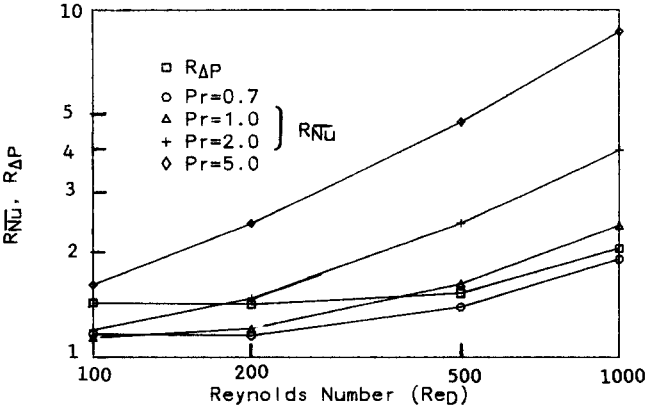

Figure 11 Effect of flow parameters for the optimum geometric parameters: $G = 0.7$, $h = 0.3$, $L = 1.2$, $S = 0.0$. Obtained with Re_D = 1,000, Pr = 1.0

with a maximum error of 11 percent. The second term on the right-hand side represents an increase in the pressure drop that occurs because of enhancement. The large influence of promoter height and annular gap is indicated by large exponents of these variables.

Nusselt-number ratio

$$R_{\overline{Nu}} = 1 + \frac{0.000222(L)^{0.062}(Re_D)^{1.017}(Pr)^{1.102}}{(L_t)^{0.50}(1-h)^{4.34}(G)^{0.60}} \quad (27)$$

with a maximum error of 8 percent. The second term on the right-hand side represents an increase in the heat transfer that occurs because of enhancement. Maximum influence of promoter height is evidenced by its large exponent.

Conclusions

Heat transfer and pressure drop in an enhanced tube annulus are higher than those in an equivalent unenhanced tube annulus. A Gaussian promoter provides higher heat transfer enhancement with a smaller increase in the pressure drop. The heat transfer is influenced primarily by the promoter height, the Reynolds number, and the Prandtl number. The pressure drop depends upon the promoter height, the annular gap, and the Reynolds number. Effects of the remaining two parameters, the promoter length and the promoter spacing, are small. In general, both the heat transfer and the pressure drop decrease as the promoter length or promoter spacing increases.

References

Agrawal, A. K. and Sengupta, S. 1987. Recirculating flow and heat transfer in an axisymmetric cavity bounded by a cylinder. *Convective Transport*, Jaluria, Y. et al. (eds.), Vol. 82. ASME HTD, New York, 1–7

Agrawal, A. K. and Sengupta, S. 1989. Fluid flow and heat transfer in blocked annuli. *Numer. Heat Transfer*, Part A, **15**, 489–508

Berner, C., Durst, F., and McEligot, D. M. 1984. Flow around baffles. *ASME J. Heat Transfer*, **106**, 743–749

Cheng, C. H. and Huang, W. H. 1991. Numerical prediction for laminar forced convection in parallel-plate channels with transverse fin arrays. *Int. J. Heat Mass Transfer*, **34**, 2739–2749

Dalle Donne, M. and Meyer, L. 1978. Turbulent convective heat transfer from rough surfaces with two-dimensional rectangular ribs. *Int. J. Heat Mass Transfer*, **20**, 583–620

Kelkar, K. M. and Patankar, S. V. 1987. Numerical prediction of flow and heat transfer in a parallel plate channel with staggered fins. *ASME J. Heat Transfer*, **109**, 25–30

Meyer, L. 1982. Thermohydraulic characteristics of single rods with three-dimensional roughness. *Int. J. Heat Mass Transfer*, **25**, 1043–1058

Obermeier, E. and Schaber, A. 1978. Experimental investigation of heat transfer from transverse finned tubes with longitudinal flow. *Proceedings of 6th International Heat Transfer Conference*. Hemisphere, Washington, DC, 613–617

Patankar, S. V. 1980. *Numerical Heat Transfer and Fluid Flow*. Hemisphere, Washington, DC

Prata, A. T. and Sparrow, E. M. 1984. Heat transfer and fluid flow characteristics for an annulus of periodically varying cross-section. *Numer. Heat Transfer*, **7**, 285–304

Rowley, G. J. and Patankar, S. V. 1984. Analysis of laminar flow and heat transfer in tubes with internal circumferential fins. *Int. J. Heat Mass Transfer*, **27**, 553–560

Webb, R. L. 1987. Enhancement of single-phase heat transfer. *Handbook of Single Phase Convective Heat Transfer*, Kakac, S., et al. (eds.). John Wiley, New York, Chapter 17